CoCrFeMnNi high-entropy alloys reinforced with Laves phase by adding Nb and Ti elements

Gang Qin[1], Zibo Li[1], Ruirun Chen[2,a)] (iD), Huiting Zheng[1], Chenlei Fan[1], Liang Wang[1],
Yanqing Su[1], Hongsheng Ding[1], Jingjie Guo[1], Hengzhi Fu[1]

[1]*National Key Laboratory for Precision Hot Processing of Metals, Harbin Institute of Technology, 150001, Harbin, China*
[2]*National Key Laboratory for Precision Hot Processing of Metals, Harbin Institute of Technology, 150001, Harbin, China; and State Key Laboratory of Advanced Welding and Joining, Harbin Institute of Technology, 150001, Harbin, China*
a)Address all correspondence to this author. e-mail: ruirunchen@hit.edu.cn

Received: 28 August 2018; accepted: 20 November 2018

Laves phase plays a positive role in improving the strength of high-entropy alloys (HEAs); Nb and Ti elements have potential to promote Laves phase formation in some HEAs. For improving the strength of the face-centered cubic (FCC) CoCrFeMnNi HEA, a series of $(CoCrFeMnNi)_{100-x}Nb_x$ (atomic ratio: $x = 0, 4, 8, 12, 16$) and $(CoCrFeMnNi)_{100-x}Ti_x$ (atomic ratio: $x = 0, 2, 4, 6, 8, 12$) HEAs were prepared by melting. The effects of Nb and Ti on the microstructure evolution and compressive properties of the CoCrFeMnNi HEAs were investigated. For $(CoCrFeMnNi)_{100-x}Nb_x$ HEAs, the second-phase (Laves and σ phase) volume fraction increased from 0 to 42%. The yield strength also increased gradually from 202 to 1010 MPa. However, the fracture strain decreased from 60% (no fracture) to 12% with increasing Nb content. For $(CoCrFeMnNi)_{100-x}Ti_x$ HEAs, the yield strength increased from 202 to 1322 MPa. The Laves phase volume fraction also increased from 0 to 27%. However, the fracture strain decreased from 60% (no fracture) to 7.5% with increasing Ti content. Addition of Nb and Ti has a good effect on improving the strength of FCC CoCrFeMnNi HEA.

Introduction

In the past few years, high-entropy alloys (HEAs) have attracted considerable research attention because of their excellent mechanical properties and simple solid solution structure. Many materials scientists have conducted a lot of research in the fields such as forging [1, 2], heat treatment [3, 4, 5], alloying [6, 7, 8], casting [9, 10], and phase stability [11]. Since 2004, when they were first proposed independently by Yeh and Cantor [12, 13], HEAs have emerged as an important breakthrough in the traditional alloy design and have opened a new path for exploring new materials with excellent properties.

The traditional alloy design involves selecting the major component based on a specific property requirement and then conferring secondary properties by using alloying addition without sacrificing the primary property [13]. Several similar methods had been used in the field of HEAs. He et al. investigated the alloying effect of Al on the phase structure, strength, and ductility of the CoCrFeMnNi HEA system and found that the Al element had potential to directly change the

phase structure and mechanical properties of CoCrFeMnNi HEA [14]. The crystal structure, microstructure, microhardness, and compression properties of $CoCrFeMnNiV_x$ ($x = 0$, 0.25, 0.5, 0.75, 1) HEAs were studied by Stepanov et al., who reported that the sigma phase volume fraction increased with increase in the V content; in CoCrFeMnNiV, they found that the sigma phase became the matrix phase [15]. In other studies, different elements (V/Nb/B/Mo/Si/Ti/Zr) were also added to AlCoCrFeNi HEA, and the alloying effect of these elements on the microstructure and mechanical properties was investigated [14, 15, 16, 17, 18, 19, 20, 21]. Table I summarizes some available literatures about the alloying effect on phase composition and mechanical properties of HEAs; the data indicate that some elements promote the formation of hard phase (body-centered cubic/Laves/δ phase) and improve the strength of alloys. In 2017 and 2018 [18, 19], Fang and his team designed two eutectic HEAs ($CoCrFeNiTa_x$ and $CoCrFeNiZr_x$ HEAs) strengthened by Laves phase; these two HEAs have excellent mechanical properties, which again proved that some elements could promote the formation of

TABLE I: Effect of some elements on the phase formation and mechanical properties of HEAs.

Basis material	Alloy element	Second phase	Yield strength	Fracture strain
CoCrFeNi [15, 20, 21]	Nb	Laves	Up	Down
CoCrFeNi [19]	Mo	δ	Up	Down
CoCrFeNi [18]	Ti	Laves	Up	Down
CoCrFeMnNi [14]	Al	BCC	Up	Down
CoCrFeMnNi [17]	V	Tetragonal	Up	Down
CoCrCuFeNi [16]	Ti	Laves	Up	Down

Laves phase and improve the strength of alloys. Low enthalpy of mixing (ΔH_{mix}) is helpful to form intermetallic in HEAs. Nb and Ti elements were added to FCC CoCrFeMnNi HEAs, which can decrease the ΔH_{mix} of $(CoCrFeMnNi)_{100-x}Nb_x$ and $(CoCrFeMnNi)_{100-x}Ti_x$ HEAs. Thus, it is possible that the addition of Nb and Ti to $(CoCrFeMnNi)_{100-x}Nb_x$ and $(CoCrFeMnNi)_{100-x}Ti_x$ HEAs induces hard phase formation in CoCrFeMnNi matrix alloy. However, based on the existing reports in the literatures [14, 15, 16, 17, 18, 19, 20, 21, 22, 23, 24, 25, 26, 27, 28], the effect of Nb and Ti addition on the structure evolution and mechanical properties of CoCrFeMnNi HEA has not been investigated thus far [14, 15, 16, 17, 18, 19, 20, 21, 22, 23, 24, 25, 26, 27, 28, 29, 30]. The gap should be filled up.

In the present study, an HEA containing CoCrFeMnNi (all elements in equal atomic proportions) with a single face-centered cubic (FCC) phase solid solution was selected as the baseline alloy system. A systematic study on the alloying effect of Nb and Ti on the microstructure, phase evolution, and mechanical properties of the $(CoCrFeMnNi)_{100-x}Nb_x$ and $(CoCrFeMnNi)_{100-x}Ti_x$ HEAs was carried out. The correlations between the microstructure and the mechanical properties of these HEAs were determined. In addition, considering the combined effects of entropy of mixing (ΔS_{mix}), enthalpy of mixing (ΔH_{mix}), atomic radius difference (Δ), valence electron concentration (VEC), and the scald ratio of ΔS_{mix} to ΔH_{mix} (Ω), we tried to reveal the relevance between the phase translation and element properties.

Results and discussion
Phase composition

As shown in Fig. 1(a), the XRD patterns of $(CoCrFeMnNi)_{100-x}Nb_x$ (x = 0, 4, 8, 12, 16, hereafter in atomic ratio) HEAs indicate a phase selection from the FCC phase to the Laves phase and σ phase structure with increasing Nb content. The XRD patterns of $(CoCrFeMnNi)_{100-x}Ti_x$ (x = 0, 2, 4, 6, 8, 12, hereafter in atomic ratio) HEAs also show a phase selection from the FCC phase to the Laves phase [see Fig. 1(b)]. This change enables the alloy system to attain a multiphase

microstructure, in which both phases obtain the maximum benefit of the solid solution strengthening effect compared with only one phase [31]. A single FCC structure was observed when the Nb content was 0. When the Nb content was 4%, only a weak reflection peak corresponding to σ phase and Laves phase structure was found. When the Nb content was 4–16%, the alloys show a multiphase (FCC, Laves phase, and σ phase) structure, which was obviously induced by the addition of Nb element. As shown in Fig. 1(b), the phase of the alloys was identified as a single FCC solid solution when the Ti content was lower (x = 0, 2, 4, 6), at which point the alloy mainly was strengthened by the solid solution strengthening mechanism. The weak reflection peak corresponding to the Laves phase and Laves* phase appeared when the Ti content reached 8 at.%. Thus, this alloy obtained a multiphase (FCC, Laves phase, and Laves* phase) structure when the Ti content was 8–12 at.%, at which point the alloy mainly was strengthened by the solid solution strengthening mechanism and the second-phase strengthening mechanism. The Ti element had a considerable influence on the phase translation from the FCC to the Laves phase structure in the alloys.

Microstructure and mechanical property

Figure 2 shows the compressive mechanical behavior of $(CoCrFeMnNi)_{100-x}Nb_x$ and $(CoCrFeMnNi)_{100-x}Ti_x$ HEAs. The compressive yield strength of the $(CoCrFeMnNi)_{100-x}Nb_x$ HEAs increased from 202 to 1010 MPa; however, the fracture strain decreased from 60% (no fracture) to 12% with the addition of Nb from 0 to 16% [see Fig. 2(a)]. Figure 2(b) shows the stress–strain curve of the compression test for the $(CoCrFeMnNi)_{100-x}Ti_x$ alloys. The yield strength of the alloys increased from 202 to 1322 MPa, whereas the fracture strain decreased from 60% (no fracture) to 7.5%, with the Ti content increased from 0 to 12 at.%. The results indicate that the addition of Nb and Ti has a positive effect on improving the strength of FCC HEAs.

Figure 3 shows the microstructures of the as-cast $(CoCrFeMnNi)_{100-x}Nb_x$ HEAs with different Nb contents, and the relationship between the yield strength and the second-phase (Laves and σ phase) volume fraction with different Nb contents in $(CoCrFeMnNi)_{100-x}Nb_x$ HEAs. Nb-0 alloys were identified by XRD (see Fig. 1) with a single FCC phase microstructure, in agreement with the previous study [14]. A small number of lath-shaped σ phase particles were generated when the Nb content was 4% [see Fig. 3(b)], at which point the alloy mainly consisted of the FCC phase. When the Nb content reached 8%, the Laves phase (eutectic structure, Nb-rich) appears and the volume increased gradually [see Figs 3(c) and 3(d)]. When the Nb content reached 16%, the alloy mainly consisted of the Laves phase [see Fig. 3(e)]. The number of
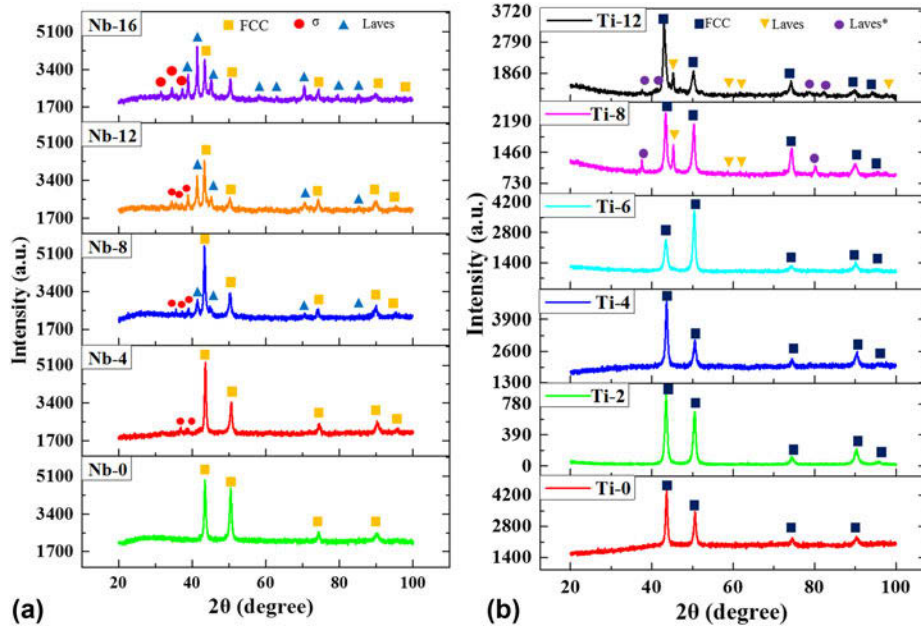
Figure 1: XRD patterns of HEAs. (a) $(CoCrFeMnNi)_{100-x}Nb_x$ and (b) $(CoCrFeMnNi)_{100-x}Ti_x$.

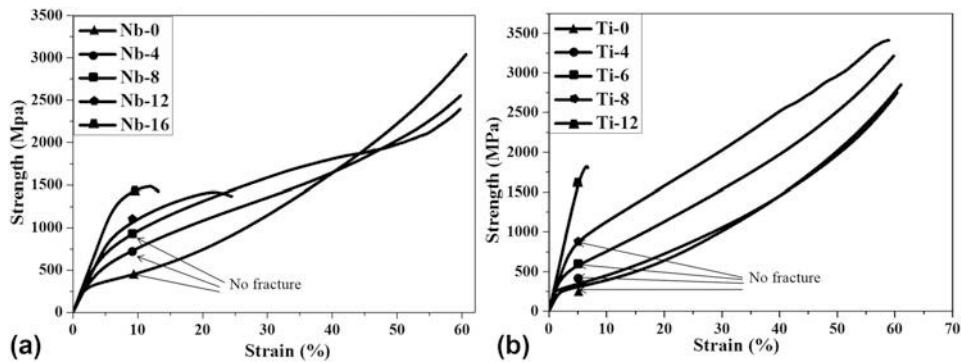**Figure 2:** Engineering stress–strain curves from compressive properties of HEAs. (a) $(CoCrFeMnNi)_{100-x}Nb_x$ (triangle, circular, quadrilateral, pentagon, and echelon represent the Nb-0, Nb-4, Nb-8, Nb-12, and Nb-16 HEAs, respectively). (b) $(CoCrFeMnNi)_{100-x}Ti_x$ (triangle, circular, quadrilateral, pentagon, and echelon represent the Ti-0, Ti-4, Ti-6, Ti-8, and Ti-12 HEAs respectively).

Laves phases increases with increasing Nb content; this encourages growth in the phase boundary density, which creates additional obstacles for dislocation slipping, thus contributing to improving the strength of the alloy. In Fig. 3 (c), the black areas indicate oxides; however, whether the oxygen was introduced through the raw material or during one of the subsequent processing steps is not known. However, because of their tiny volume fracture, they did not significantly influence mechanical properties, which is not surprising since they also have been previously found in these alloys [32, 33, 34, 35]. Figure 3(f) shows the relationship between the yield strength and the second-phase (Laves and σ phase) volume fraction with different Nb contents in $(CoCrFeMnNi)_{100-x}Nb_x$ HEAs. The second-phase volume fraction increased with increase in Nb content. The yield strength also increased as

the second-phase volume fraction increased from 0 to 42%. This indicates that the increase in the second phase induced by adding Nb is the key factor for the improvement of the yield strength in this HEA system. In addition, the previous studies [16, 17, 20, 21, 23, 25, 29] also reported that Nb/Ti addition to CoCrFeNi/CoCrCuFeNi/AlCoCrFeNi HEAs, which also show the same result that Laves phase was generated in these HEAs. It proves that Nb and Ti elements have a positive effect on forming Laves phase, improving the strength of these HEAs.

Figures 4(a)–4(e) show the microstructure morphology of the as-cast $(CoCrFeMnNi)_{100-x}Ti_x$ ($x = 0, 4, 6, 8, 12$) HEAs. As shown in Fig. 4(a), combined with the XRD pattern in Fig. 1(b), the Ti-0 alloy (Ti content of 0 at.%) presented a single FCC phase structure. Some Laves phases (Ti segregation particles)
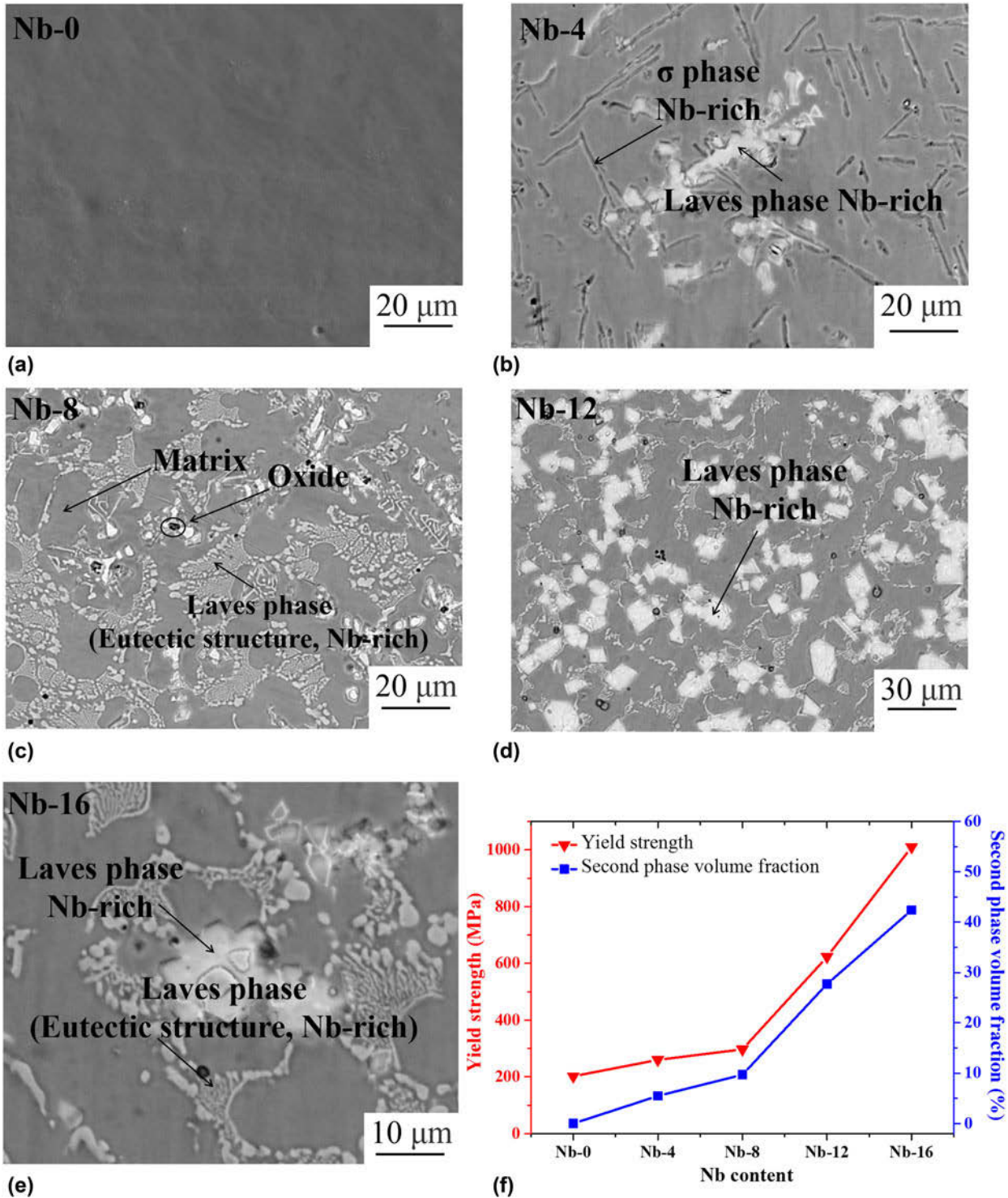
Figure 3: Back scattered-electron (SEM-BSE) microstructure and yield strength of $(CoCrFeMnNi)_{100-x}Nb_x$ alloys. (a) $x = 0$, (b) $x = 4$, (c) $x = 8$, (d) $x = 12$, (e) $x = 16$, (f) relationship between the yield strength and the second-phase volume fraction.

were observed in the Ti-4 alloy, as shown in Fig. 4(b). When the Ti content was 6%, a small number of Laves* phases were observed in the Ti-6 alloy. The volume fraction of the new Laves* phase increased with increase in the Ti content [see Figs. 4(c)–4(e)]. Figure 4(f) shows the yield strength and the second-phase (Laves phase and Laves* phase) volume fraction with different Ti contents in the $(CoCrFeMnNi)_{100-x}Ti_x$ HEAs. The second-phase volume fraction increased from 0 to 27% as
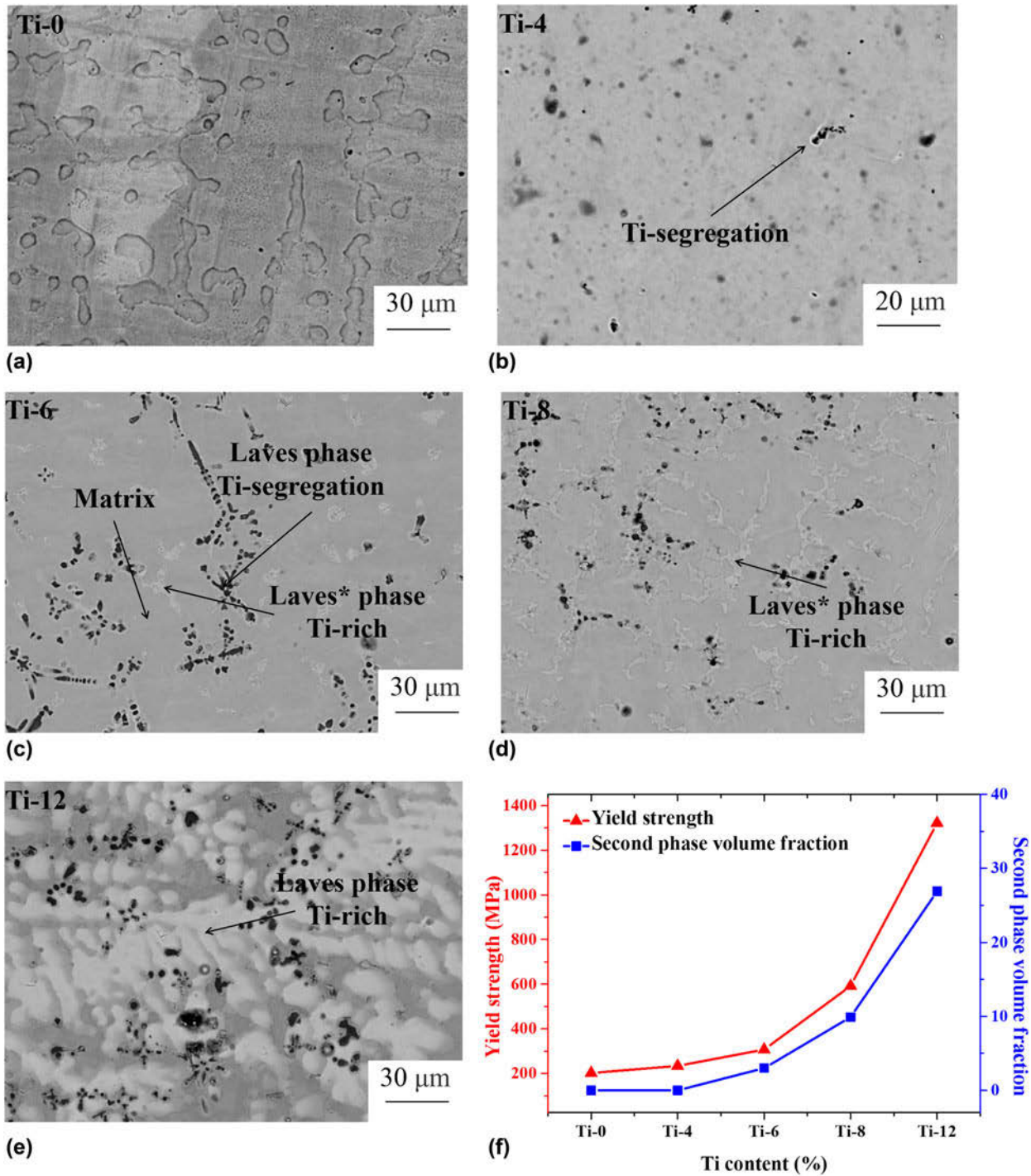
Figure 4: Microstructure and yield strength of $(CoCrFeMnNi)_{100-x}Ti_x$ alloys. (a) $x = 0$, (b) $x = 4$, (c) $x = 6$, (d) $x = 8$, (e) $x = 12$, (f) the yield strength and the second-phase volume fraction.

the Ti content increased. The yield strength also increased with the increase in the second-phase volume fraction, which indicates the second phase induced by the addition of Ti is the key factor for increasing the yield strength.

The FCC phase structure has better plasticity and low strength, whereas the Laves phase has higher strength and

limited plasticity. The yield strength of the alloys can be estimated by the simple rule of mixtures [Eq. (1)] [36, 37, 38, 39].

$$\delta = \delta_{fcc} V_{fcc} + \delta_{Laves} \cdot V_{Laves} \quad , \qquad (1)$$

where δ_{fcc} and δ_{Laves} denote the strength of the FCC and the Laves phase, respectively, and V_{fcc} and V_{Laves} refer to the volume fraction

of the FCC and the Laves phase, respectively. This implies that the strength and plasticity can be regulated based on practical application by changing the alloy element (Nb and Ti) content.

The elemental distribution is done by Energy Dispersive Spectrometer (EDS), and the compositions (at.%) of various phases in as-cast $(CoCrFeMnNi)_{84}Nb_{16}$ and $(CoCrFeMnNi)_{92}Ti_8$ HEAs are shown in Table II, which indicates the composition distribution in the $(CoCrFeMnNi)_{84}Nb_{16}$ HEA. In $(CoCrFeMnNi)_{84}Nb_{16}$ HEA, the Laves phase is shown to be an Nb-rich region, whereas the FCC phase is an Nb-poor region. The Laves phase and Laves* phase in the $(CoCrFeMnNi)_{92}Ti_8$ HEA are shown to be a Ti-rich region. The results prove that the Nb and Ti elements have a considerable influence on the phase selection from FCC to Laves phase structure in the alloys.

The atomic radius, entropy of mixing, and enthalpy of mixing have been proposed to predict the structural stability and phase formation in HEAs [38, 39, 40, 41, 42, 43, 44, 45, 46, 47, 48, 49, 50, 51, 52, 53, 54, 55, 56, 57]. Considering from the electronic level, VEC or the itinerant electrons per atom ratio (e/a) is an important parameter for the atom arrangement. Guo et al. proposed this parameter for predicting phase formation and summed up the correlation of VEC and FCC/BCC phase formation. FCC phases have been found to be stable at higher VEC (≥ 8), whereas BCC phases are stable at lower VEC (<6.87) in HEAs [41, 42, 43]. Tsai et al. proposed that alloys having VEC values between 6.88 and 7.84 are prone to σ phase formation either in the as-cast state or during aging at suitable temperatures [43, 44]. They provided an important reference for the design of HEA. The value of VEC can be attained by Eq. (2) [41, 42, 43, 44].

$$VEC = \sum_{i=1}^{n} C_i(VEC)_i \quad , \qquad (2)$$

where C_i is the atom percentage and $(VEC)_i$ is the VEC for the ith element.

Based on the correlation between VEC and the FCC/BCC phase, a function about the VEC and the content of Nb and Ti element was established. As shown in Fig. 5, VEC decreased with increasing Nb and Ti content because of the VEC values

of the Nb and Ti were lower than the average VEC of the CoCrFeMnNi HEA. Contrary to previous reports [41, 42], no BCC phase formed in this alloy system; however, Laves phase and σ phase were generated in this alloy, which agrees with the criterion proposed by Tsai for σ phase formation [43, 44].

Enthalpy of mixing (ΔH_{mix}), atomic radius difference (δ), entropy of mixing (ΔS_{mix}), and the scald ratio of ΔS_{mix} to ΔH_{mix} (Ω) are important parameters for phase selection in HEAs based on the previous reports [41, 42, 43, 44, 45, 46, 47, 48, 49, 50, 51, 52, 53, 54, 55, 56, 57]. Guo suggested that solid solution is expected if all the three parameters satisfy the conditions of $-22 \leq \Delta H_{mix} \leq 7$ kJ/mol, $0 \leq \delta \leq 8.5$, and $11 \leq \Delta S_{mix} \leq 19.5$ J/K mol [41]. Figure 6(a) shows the enthalpy of mixing (ΔH_{mix}) of $(CoCrFeMnNi)_{100-x}Nb_x$ HEAs and $(CoCrFeMnNi)_{100-x}Ti_x$ HEAs. The ΔH_{mix} can be estimated by Eq. (3) [54].

$$\Delta H_{mix} = \sum_{n=1}^{n} \Omega_{ij} c_i c_{ji \neq j} \quad , \qquad (3)$$

where Ω_{ij} usually equals to $4 \Delta H_{ij}^{mix}$ and ΔH_{ij}^{mix} is the enthalpy of mixing of the ith and jth component element [54, 55, 57].

It shows that the ΔH_{mix} of both $(CoCrFeMnNi)_{100-x}Nb_x$ and $(CoCrFeMnNi)_{100-x}Ti_x$ HEAs decreases with increasing Nb/Ti content. The value of ΔH_{mix} is less than zero, which indicates that the reaction is an exothermic reaction. In the process of alloy solidification, the temperature decreases, which is helpful to promote the reaction and form intermetallic. The lower the mixing enthalpy is, the higher the probability of the chemical reaction.

Figure 6(b) shows the atomic radius difference (δ) of $(CoCrFeMnNi)_{100-x}Nb_x$ HEAs and $(CoCrFeMnNi)_{100-x}Ti_x$ HEAs. The atomic radius difference (δ) was calculated by Eq. (4) [14, 52, 53, 54, 55, 56, 57].

$$\delta = \sqrt{\sum_{n=1}^{n} c_i \left(1 - r_i \Big/ \sum_{n=1}^{n} (c_i r_i) \right)^2} \quad . \qquad (4)$$

It shows that δ of both HEAs increases with increasing Nb/Ti content. The large lattice distortion energy, induced by Nb/Ti addition, can be released by the method of phase translation,

TABLE II: Compositions (at.%) of various phases in as-cast $(CoCrFeMnNi)_{84}Nb_{16}$ and $(CoCrFeMnNi)_{92}Ti_8$ HEAs.

HEA	Region	Co	Cr	Fe	Mn	Ni	Nb/Ti
$(CoCrFeMnNi)_{84}Nb_{16}$	Nominal	16.8	16.8	16.8	16.8	16.8	16
	Laves phase (eutectic structure)	20.76	14.97	15.19	14.80	20.40	13.89
	Laves phase Nb-rich	15.15	15.33	12.17	5.64	10.91	40.8
	Matrix	20.54	21.71	21.82	14.52	19.76	1.66
CoCrFeMnNi)$_{92}$Ti$_8$	Nominal	18.4	18.4	18.4	18.4	18.4	8
	Laves* phase	20.31	13.00	13.92	9.58	20.66	22.54
	Laves phase	5.48	...	3.88	4.10	6.14	82.23
	Matrix	19.21	17.99	17.19	12.09	24.02	9.5

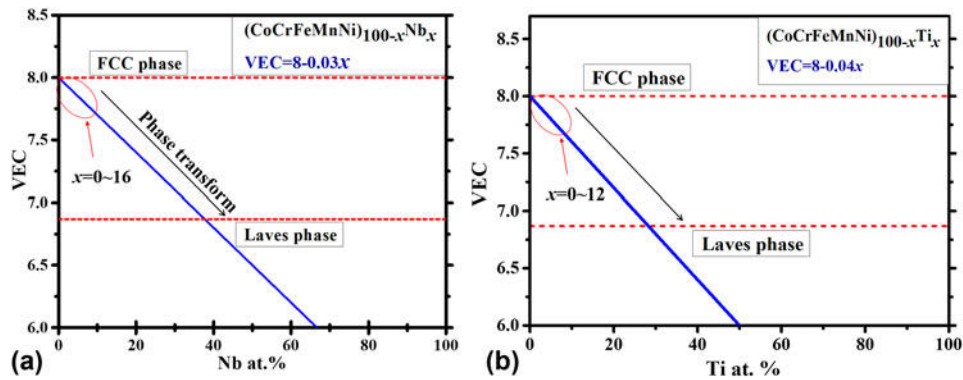Figure 5: VEC of HEAs. (a) $(CoCrFeMnNi)_{100-x}Nb_x$ and (b) $(CoCrFeMnNi)_{100-x}Ti_x$.

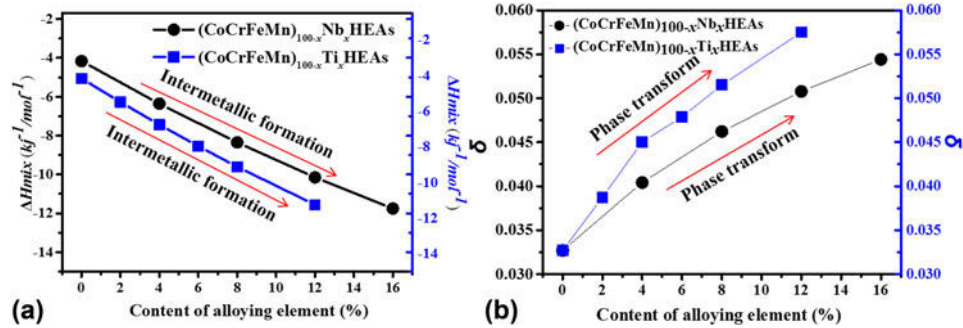Figure 6: Enthalpy of mixing (ΔH_{mix}) and atomic radius difference (Δ). (a) ΔH_{mix} and (b) δ.

so the increase of δ is helpful to promote phase translation in HEAs [14, 52, 53, 54, 55, 56].

Figure 7(a) shows the entropy of mixing (ΔS_{mix}) of $(CoCrFeMnNi)_{100-x}(Nb/Ti)_x$ HEAs. The ΔS_{mix} was attained by Eq. (5) [48, 49, 50].

$$\Delta S_{mix} = -R \sum_{n=1}^{n} (c_i \ln c_i) \quad , \quad (5)$$

where n represents the number of component elements, c_i represents the at.% of the ith component element, and R is the universal gas constant [8.314 k/(J mol)] [48, 49, 50]. It is shown that the value of ΔS_{mix} decreases with increasing Nb/Ti content, which is helpful to promote solid solution formation based on the previous reports [48, 49, 50].

The scald ratio of ΔS_{mix} to ΔH_{mix} (Ω) was pointed out as an important parameter for prediction of solid solution formation by Yang et al. and Guo et al. [40, 41]. Figure 7(b) shows the scald ratio of ΔS_{mix} to ΔH_{mix} (Ω) of $(CoCrFeMnNi)_{100-x}Nb_x$ HEAs and $(CoCrFeMnNi)_{100-x}Ti_x$ HEAs. The Ω was attained by Eq. (6) [40, 41].

$$\Omega = \frac{\sum_{n=1}^{n} (c_i(T_m)_i)\Delta S_{mix}}{|\Delta H_{mix}|} \quad , \quad (6)$$

where $(T_m)_i$ is the melting point of the ith constituent element, and it can be attained by Eq. (7) [40, 41].

$$T_m = \sum_{n=1}^{n} (c_i(T_m)_i) \quad . \quad (7)$$

Figure 7(b) shows that Ω of both HEAs increases with increasing Nb/Ti content, which plays a positive role in promoting solid solution formation based on the previous reports [40, 41].

When Nb element is added to the CoCrFeMnNi HEA, part of the Nb atoms were incorporated into the CoCrFeMnNi matrix and form FCC phase, whereas remnant Nb atoms will solid solute with other elements each other and form Laves phase finally. With increase in Nb content, part of FCC phase changes to Laves phase, and the Laves phase volume fraction increases with further increase in Nb.

Conclusions

In this study, the alloying effects of Nb and Ti elements on the microstructure evolution and compressive properties of CoCrFeMnNi HEAs were investigated. Based on the experimental and analytical results, the following conclusions were obtained:

(1) Nb and Ti have the capacity to promote the phase selection from the FCC to the Laves phase.

(2) The second-phase (Laves and σ phase) volume fraction of $(CoCrFeMnNi)_{100-x}Nb_x$ HEAs increases from 0 to

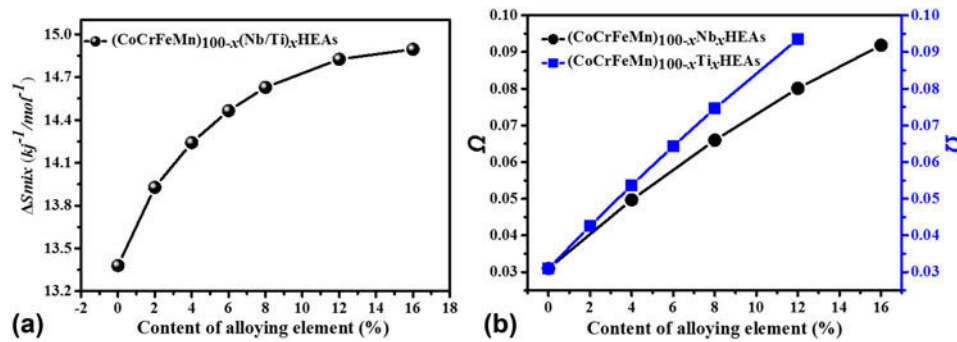**Figure 7:** Entropy of mixing (ΔS_{mix}) and the scald ratio (Ω, the ratio of ΔS_{mix} to ΔH_{mix}). (a) ΔS_{mix} and (b) Ω.

42% when Nb content is increased from 0 to 16 at.%. The second-phase (Laves phase and Laves* phase) volume fraction of $(CoCrFeMnNi)_{100-x}Ti_x$ HEAs increases from 0 to 27% with increasing Ti content from 0 to 12 at.%.

(3) The yield strength of $(CoCrFeMnNi)_{100-x}Nb_x$ HEA increases gradually from 202 to 1010 MPa with the addition of Nb at 0–16 at.%. The yield strength of $(CoCrFeMnNi)_{100-x}Ti_x$ HEAs increases gradually from 202 to 1322 MPa with the addition of Ti at 0–12 at.%.

(4) As a reinforced phase, the Laves phase is beneficial for improving the yield strength of HEAs. The increased volume fraction of Laves phase plays a positive role in improving the strength of CoCrFeMnNi HEA.

Experimental

A series of $(CoCrFeMnNi)_{100-x}Nb_x$ and $(CoCrFeMnNi)_{100-x}Ti_x$ HEAs were synthesized by arc melting a mixture of pure metals (purity >99%) in a high-purity argon atmosphere. The alloys were melted seven times for composition homogeneity. The phase structure was identified by X-ray diffraction (XRD; Empyrean) with a step size of 0.026°. Microstructure was characterized by scanning electron microscopy (SEM) with the use of a Zeiss Supra 55 instrument (Carl Zeiss AG, Oberkochen, Germany) operated at 15 kV. Element distribution was measured with an electronic probe. For microstructure observation, the SEM samples were cut from the center of the ingot. These samples were sequentially ground and polished, followed by electropolishing in a mixture of 90% acetic acid and 10% perchloric acid at room temperature and supplied with the voltage of 27 V for 15 s. Samples with dimensions of Ø4 mm × 6 mm were prepared for compressive testing; at least three specimens were tested for each same composition sample to obtain reliable results. Compression tests were carried out on an AG-X plus 250 kN electronic universal material testing machine (Shimadzu, Kyoto, Japan) at a strain rate of 0.5×10^{-3} mm/min at room temperature.

Acknowledgment

References

1. **S.J. Sun, Y.Z. Tian, H.R. Lin, X.G. Dong, Y.H. Wang, Z.J. Zhang, and Z.F. Zhang**: Enhanced strength and ductility of bulk CoCrFeMnNi high entropy alloy having fully recrystallized ultrafine-grained structure. *Mater. Des.* **133**, 122 (2017).

2. **S.J. Sun, Y.Z. Tian, H.R. Lin, H.J. Yang, X.G. Dong, Y.H. Wang, and Z.F. Zhang**: Transition of twinning behavior in CoCrFeMnNi high entropy alloy with grain refinement. *Mater. Sci. Eng., A* **712**, 603 (2018).

3. **Y. Ma, Q. Wang, C. Li, L. Santodonato, M. Feygenson, C. Dong, and P.K. Liaw**: Chemical short-range orders and the induced structural transition in high-entropy alloys. *Scr. Mater.* **64**, 144 (2018).

4. **W.Q. Wu, S. Ni, Y. Liu, and M. Song**: Effects of cold rolling and subsequent annealing on the microstructure of a HfNbTaTiZr high-entropy alloy. *J. Mater. Res.* **31**, 3815 (2016).

5. **Y. Zhang, Y. Liu, and T.X. Li**: Microstructure and mechanical properties of a refractory HfNbTiVSi₀.₅ high-entropy alloy composite. *Mater. Lett.* **174**, 82 (2016).

6. **Y. Liu, Y. Zhang, H. Zhang, N.J. Wang, X. Chen, H.W. Zhang, and Y.X. Li**: Microstructure and mechanical properties of refractory HfMo₀.₅NbTiV₀.₅Siₓ high-entropy composites. *J. Alloys Compd.* **694**, 869 (2017).

7. **Y. Liu, M. Chen, Y.X. Li, and X. Chen**: Microstructure and mechanical performance of AlₓCoCrCuFeNi high-entropy alloys. *Rare Met. Mater. Eng.* **38**, 602 (2009).

8. **X.W. Liu, L. Liu, G. Liu, X.X. Wu, D.H. Lu, J.Q. Yao, W.M. Jiang, Z.T. Fan, and W.B. Zhang**: The role of carbon in grain refinement of cast CrFeCoNi high-entropy alloys. *Metall. Mater. Trans. A* **49**, 2151 (2018).

9. **Y.P. Lu, Y. Dong, S. Guo, L. Jiang, H.J. Kang, T.M. Wang, B. Wen, Z.J. Wang, J.C. Jie, Z.Q. Cao, H.H. Ruan, and T.J. Li**: A

promising new class of high-temperature alloys: Eutectic high-entropy alloys. *Sci. Rep.* **4**, 6200 (2014).

10. Y.P. Lu, X.Z. Gao, L. Jiang, Z.N. Chen, T.M. Wang, J.C. Jie, H.J. Kang, Y.B. Zhang, S. Guo, H.H. Ruan, Y.H. Zhao, Z.Q. Cao, and T.J. Li: Directly cast bulk eutectic and near-eutectic high entropy alloys with balanced strength and ductility in a wide temperature range. *Acta Mater.* **124**, 143 (2017).

11. J.Q. Yao, X.W. Liu, N. Gao, Q.H. Jiang, N. Li, G. Liu, W.B. Zhang, and Z.T. Fan: Phase stability of a ductile single-phase BCC Hf$_{0.5}$Nb$_{0.5}$Ta$_{0.5}$Ti$_{1.5}$Zr refractory high-entropy alloy. *Intermetallics* **98**, 79 (2018).

12. J.W. Yeh, S.K. Chen, S.J. Lin, J.Y. Gan, T.S. Chin, T.T. Shun, C.H. Tsau, and S.Y. Chang: Nanostructured high-entropy alloys with multiple principal elements: Novel alloy design concepts and outcomes. *Adv. Eng. Mater.* **6**, 299 (2004).

13. B. Cantor, I.T.H. Chang, P. Knight, and A.J.B. Vincent: Microstructural development in equiatomic multicomponent alloys. *Mater. Sci. Eng., A* **213**, 375 (2004).

14. J.Y. He, W.H. Liu, H. Wang, Y. Wu, X.J. Liu, T.G. Nieh, and Z.P. Lu: Effects of Al addition on structural evolution and tensile properties of the FeCoNiCrMn high-entropy alloy system. *Acta Mater.* **62**, 105 (2014).

15. N.D. Stepanov, D.G. Shaysultanov, G.A. Salishchev, M.A. Tikhonovsky, E.E. Oleynik, A.S. Tortika, and O.N. Senkov: Effect of V content on microstructure and mechanical properties of the CoCrFeMnNiV$_x$ high entropy alloys. *J. Alloys Compd.* **628**, 170 (2015).

16. W.H. Liu, J.Y. He, H.L. Huang, H. Wang, Z.P. Lu, and C.T. Liu: Effects of Nb additions on the microstructure and mechanical property of CoCrFeNi high-entropy alloys. *Intermetallics* **60**, 1 (2015).

17. X.F. Wang, Y. Zhang, Y. Qiao, and G.L. Chen: Novel microstructure and properties of multicomponent CoCrCuFeNiTi$_x$, alloys. *Intermetallics* **15**, 357 (2007).

18. W.Y. Huo, H. Zhou, F. Fang, Z.H. Xie, and J.Q. Jiang: Microstructure and mechanical properties of CoCrFeNiZr$_x$ eutectic high-entropy alloys. *Mater. Des.* **134**, 226 (2017).

19. W.Y. Huo, H. Zhou, F. Fang, X.F. Zhou, Z.H. Xie, and J.Q. Jiang: Microstructure and properties of novel CoCrFeNiTa$_x$ eutectic high-entropy alloys. *J. Alloys Compd.* **735**, 897 (2018).

20. T.T. Shun, L.Y. Chang, and M.H. Shiu: Microstructures and mechanical properties of multiprincipal component CoCrFeNiTi$_x$ alloys. *Mater. Sci. Eng., A* **556**, 170 (2012).

21. W.H. Liu, Z.P. Lu, J.Y. He, J.H. Luan, Z.J. Wang, B. Liu, Y. Liu, M.W. Chen, and C.T. Liu: Ductile CoCrFeNiMo$_x$ high entropy alloys strengthened by hard intermetallic phases. *Acta Mater.* **116**, 332 (2016).

22. H. Jiang, L. Jiang, D.X. Qiao, Y.P. Lu, T.M. Wang, Z.Q. Cao, and T.J. Li: Effect of niobium addition on microstructure and properties of the CoCrFeNb$_x$Ni high entropy alloys. *J. Mater. Sci. Technol.* **33**, 712 (2016).

23. F. He, Z. Wang, P. Cheng, Q. Wang, J.J. Li, Y.Y. Dang, J.C. Wang, and C.T. Liu: Designing eutectic high entropy alloys of CoCrFeNiNb$_x$. *J. Alloys Compd.* **656**, 284 (2016).

24. Y. Dong, K.Y. Zhou, Y.P. Lu, X.X. Gao, T.M. Wang, and T.J. Li: Effect of vanadium addition on the microstructure and properties of AlCoCrFeNi high entropy alloy. *Mater. Des.* **57**, 67 (2015).

25. S.G. Ma and Y. Zhang: Effect of Nb addition on the microstructure and properties of AlCoCrFeNi high-entropy alloy. *Mater. Sci. Eng., A* **532**, 480 (2012).

26. Q.S. Chen, Y.P. Lu, Y. Dong, T.M. Wang, and T.J. Li: Effect of minor B addition on microstructure and properties of AlCoCrFeNi multi-component alloy. *Trans. Nonferrous Met. Soc. China* **25**, 2958 (2015).

27. J.M. Zhu, H.F. Zhang, H.M. Fu, A.M. Wang, H. Li, and Z.Q. Hu: Microstructures and compressive properties of multicomponent AlCoCrCuFeNiMo$_x$ alloys. *J. Alloys Compd.* **497**, 52 (2010).

28. J.M. Zhu, H.M. Fu, H.F. Zhang, A.M. Wang, H. Li, and Z.Q. Hu: Synthesis and properties of multiprincipal component AlCoCrFeNiSi$_x$ alloys. *Mater. Sci. Eng., A* **527**, 7210 (2010).

29. Y. Yu, J. Wang, J.S. Li, H.C. Kou, and W.M. Liu: Characterization of BCC phases in AlCoCrFeNiTi$_x$ high entropy alloys. *Mater. Lett.* **138**, 78 (2015).

30. J. Chen, P. Niu, Y. Liu, Y.Y. Lu, X.H. Wang, Y.L. Peng, and J.N. Liu: Effect of Zr content on microstructure and mechanical properties of AlCoCrFeNi high entropy alloy. *Mater. Des.* **94**, 39 (2016).

31. Z.M. Li, K.G. Pradeep, and Y. Deng: Metastable high-entropy dual-phase alloys overcome the strength–ductility trade-off. *Nature* **534**, 227 (2016).

32. F. Otto, A. Dlouhý, K.G. Pradeep, M. Kuběnová, D. Raabe, G. Eggeler, and E.P. George: Decomposition of the single-phase high-entropy alloy CrMnFeCoNi after prolonged anneals at intermediate temperatures. *Acta Mater.* **112**, 40 (2016).

33. A. Gali and E.P. George: Tensile properties of high- and medium-entropy alloys. *Intermetallics* **39**, 74 (2013).

34. F. Otto, N.L. Hanold, and E.P. George: Microstructural evolution after thermo mechanical processing in an equiatomic, single-phase CoCrFeMnNi high entropy alloy with special focus on twin boundaries. *Intermetallics* **54**, 39 (2014).

35. X. Chen, Y.W. Sui, J.Q. Qi, Y.Z. He, F.X. Wei, Q.K. Meng, and Z. Sun: Microstructure of Al$_{1.3}$CrFeNi eutectic high entropy alloy and oxidation behavior at 1000 °C. *J. Mater. Res.* **11**, 32 (2017).

36. Y.J. Zhou, Y. Zhang, Y.L. Wang, and G.L. Chen: Solid solution alloys of AlCoCrFeNiTi$_x$ with excellent room-temperature mechanical properties. *Appl. Phys. Lett.* **90**, 253 (2007).

37. S.W. Tsai: *Theory of Composites Design* (Think Composites Press, San Francisco, 1992).

38. Y. Zhang, Y. Zhou, J. Lin, G. Chen, and P.K. Liaw: Solid-solution phase formation rules for multi-component alloys. *Adv. Eng. Mater.* **10**, 534 (2008).

39. **T. Egami and Y. Waseda**: Atomic size effect on the formability of metallic glasses. *J. Non-Cryst. Solids* **64**, 113 (1984).

40. **X. Yang and Y. Zhang**: Prediction of high-entropy stabilized solid-solution in multi-component alloys. *Mater. Chem. Phys.* **132**, 233 (2012).

41. **S. Guo and C.T. Liu**: Phase stability in high entropy alloys: Formation of solid-solution phase or amorphous phase. *Prog. Nat. Sci.: Mater. Int.* **21**, 433 (2011).

42. **S. Guo, C. Ng, J. Lu, and C.T. Liu**: Effect of valence electron concentration on stability of fcc or bcc phase in high entropy alloys. *J. Appl. Phys.* **109**, 645 (2011).

43. **M.H. Tsai, K.Y. Tsai, C.W. Tsai, C. Lee, C.C. Juan, and J.W. Ye**: Criterion for sigma phase formation in Cr- and V-containing high-entropy alloys. *Mater. Res. Lett.* **1**, 207 (2013).

44. **M.H. Tsai, K.C. Chang, J.H. Li, R.C. Tsai, and A.H. Cheng**: A second criterion for sigma phase formation in high-entropy alloys. *Mater. Res. Lett.* **4**, 1 (2016).

45. **M.C. Troparevsky, J.R. Morris, P.R.C. Kent, A.R. Lupini, and G.M. Stocks**: Criteria for predicting the formation of single-phase high-entropy alloys. *Phys. Rev. X* **5**, 1 (2015).

46. **N. Yurchenko, N. Stepanov, and G. Salishchev**: Laves-phase formation criterion for high-entropy alloys. *Met. Sci. J.* **33**, 17 (2016).

47. **O.N. Senkov and D.B. Miracle**: A new thermodynamic parameter to predict formation of solid solution or intermetallic phases in high entropy alloys. *J. Alloys Compd.* **658**, 603 (2016).

48. **B.S. Murty, J.W. Yeh, and S. Ranganathan**: *High Entropy Alloys* (Elsevier, London, 2014).

49. **Y. Zhang, T.T. Zuo, Z. Tang, M.C. Gao, K.A. Dahmen, P.K. Liaw, and Z.P. Lu**: Microstructures and properties of high-entropy alloys. *Prog. Mater. Sci.* **61**, 1 (2011).

50. **S. Guo, Q. Hu, C. Ng, and C.T. Liu**: More than entropy in high-entropy alloys: Forming solid solutions or amorphous phase. *Intermetallics* **41**, 96 (2013).

51. **Y. Zhang, X. Yang, and P.K. Liaw**: Alloy design and properties optimization of high entropy alloys. *JOM* **64**, 830 (2012).

52. **R.R. Chen, G. Qin, H.T. Zheng, L. Wang, Y.Q. Su, Y.L. Chiu, H.S. Ding, J.J. Guo, and H.Z. Fu**: Composition design of high entropy alloys using the valence electron concentration to balance strength and ductility. *Acta Mater.* **144**, 129 (2018).

53. **G. Qin, W.T. Xue, C.L. Fan, R.R. Chen, L. Wang, Y.Q. Su, H.S. Ding, and J.J. Guo**: Effect of Co content on phase formation and mechanical properties of $(AlCoCrFeNi)_{100-x}Co_x$ high-entropy alloys. *Mater. Sci. Eng., A* **710**, 200 (2018).

54. **G. Qin, S. Wang, R.R. Chen, X. Gong, L. Wang, Y.Q. Su, J.J. Guo, and H.Z. Fu**: Microstructures and mechanical properties of Nb-alloyed CoCrCuFeNi high-entropy alloys. *J. Mater. Sci. Technol.* **34**, 365 (2018).

55. **R. Feng, M.C. Gao, C. Lee, M. Mathes, T.T. Zuo, S.Y. Chen, J.A. Hawk, Y. Zhang, and P.K. Liaw**: Design of light-weight high-entropy alloys. *Entropy* **18**, 333 (2016).

56. **Y. Zhang, Z.P. Lu, S.G. Ma, P.K. Liaw, Z. Tang, Y.Q. Cheng, and M.C. Gao**: Guidelines in predicting phase formation of high-entropy alloys. *MRS Commun.* **42**, 57 (2014).

57. **B. Chanda and J. Das**: Composition dependence on the evolution of nanoeutectic in $CoCrFeNiNb_x$ ($0.45 \leq x \leq 0.65$) high entropy alloys. *Adv. Eng. Mater.* **20**, 1700908 (2018).